

**FORCE TESTS OF STANDARD HYPERVELOCITY
BALLISTIC MODELS HB-1 AND HB-2
AT MACH 1.5 TO 10**

**PROPERTY OF U.S. AIR FORCE
AEDC TECHNICAL LIBRARY**

By

**J. Don Gray and E. Earl Lindsay
von Kármán Gas Dynamics Facility
ARO, Inc.**

TECHNICAL DOCUMENTARY REPORT NO. AEDC-TDR-63-137

August 1963

AFSC Program Area 040A

**(Prepared under Contract No. AF 40(600)-1000 by ARO, Inc.,
contract operator of AEDC, Arnold Air Force Station, Tenn.)**

**ARNOLD ENGINEERING DEVELOPMENT CENTER
AIR FORCE SYSTEMS COMMAND
UNITED STATES AIR FORCE**

NOTICES

Qualified requesters may obtain copies of this report from ASTIA. Orders will be expedited if placed through the librarian or other staff member designated to request and receive documents from ASTIA.

When Government drawings, specifications or other data are used for any purpose other than in connection with a definitely related Government procurement operation, the United States Government thereby incurs no responsibility nor any obligation whatsoever; and the fact that the Government may have formulated, furnished, or in any way supplied the said drawings, specifications, or other data, is not to be regarded by implication or otherwise as in any manner licensing the holder or any other person or corporation, or conveying any rights or permission to manufacture, use, or sell any patented invention that may in any way be related thereto.

Errata AEDC-TDR-63-137, August 1963*

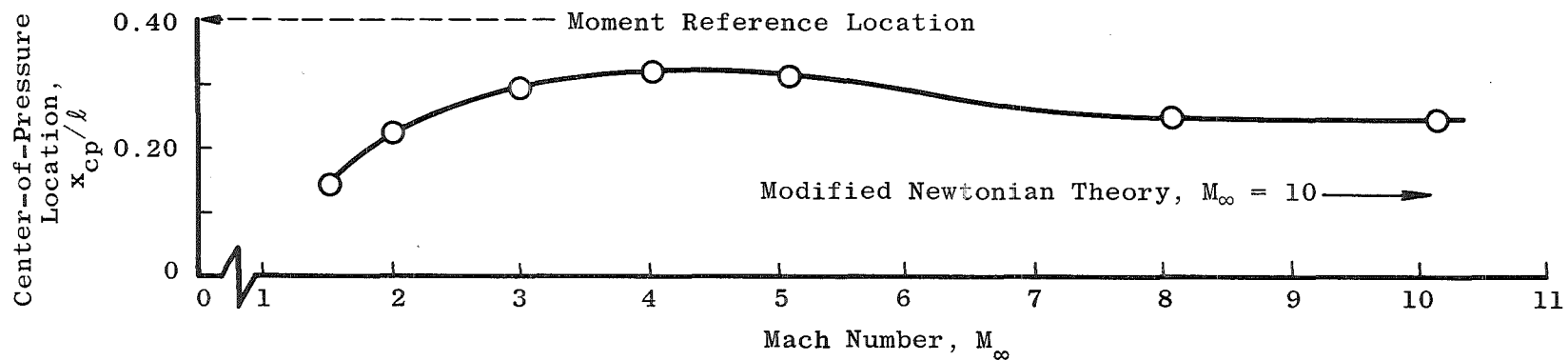
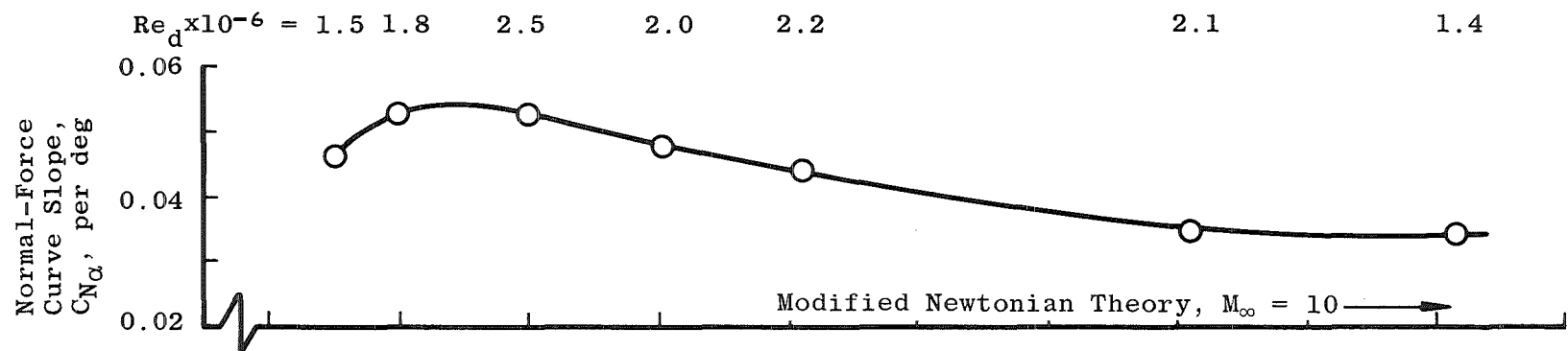
Please note the following corrections:

On page 7 the first conclusion should be changed to

1. The forebody axial-force coefficient was found to decrease with angle of attack at Mach numbers less than 3 and to increase with angle of attack at all larger Mach numbers.

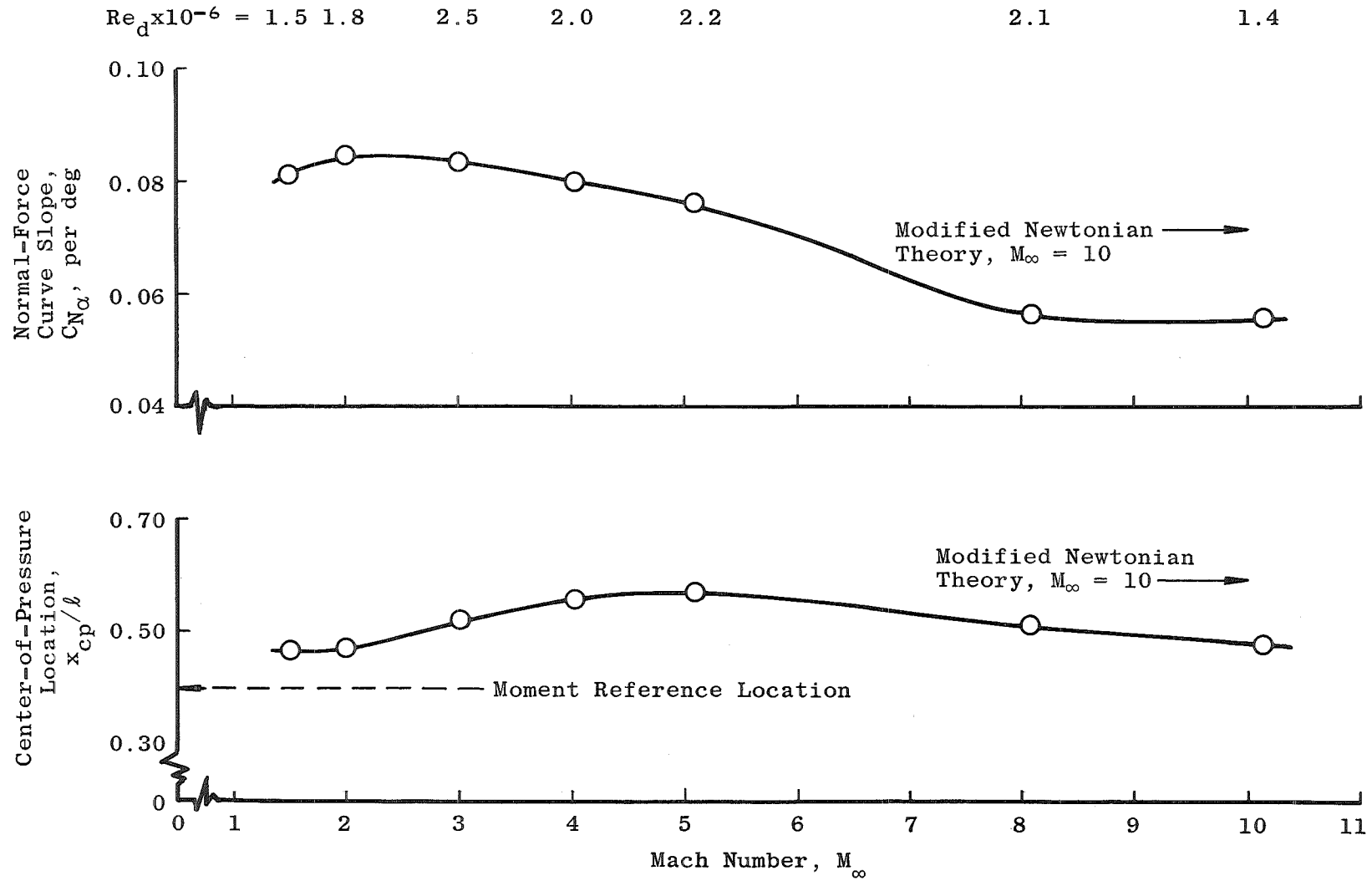
The attached pages should be substituted for pp. 27 and 28, Figs. 10a and b and p. 30, Fig. 11b.

*J. Don Gray and E. Earl Lindsay. "Force Tests of Standard Hypervelocity Ballistic Models HB-1 and HB-2 at Mach 1.5 to 10." Arnold Engineering Development Center, Arnold Air Force Station, Tennessee. AEDC-TDR-63-137, August 1963. (Unclassified Report)



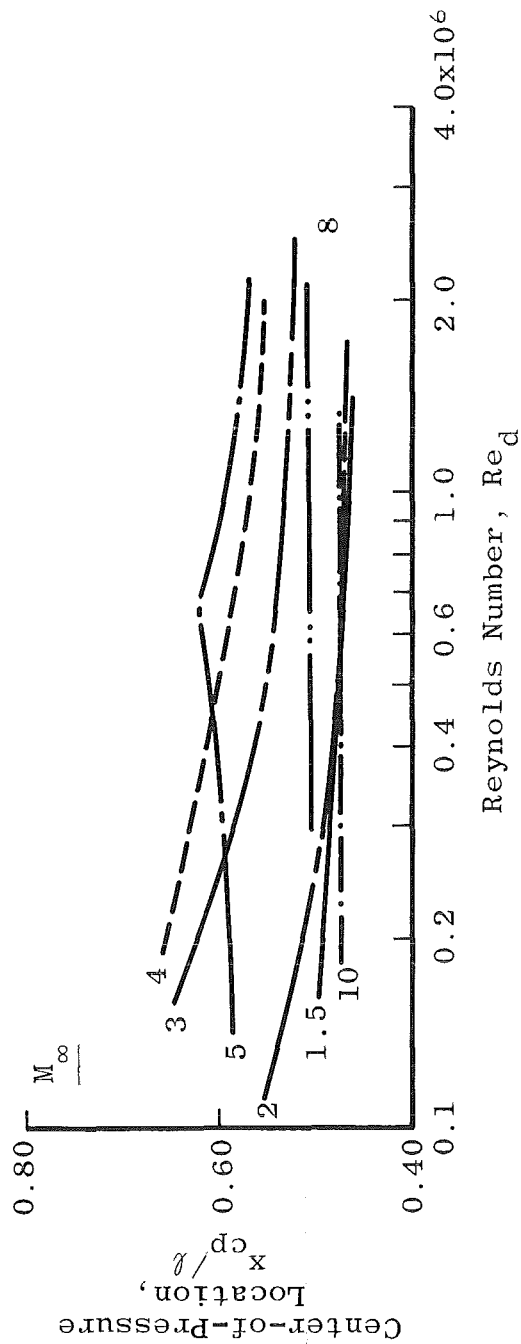
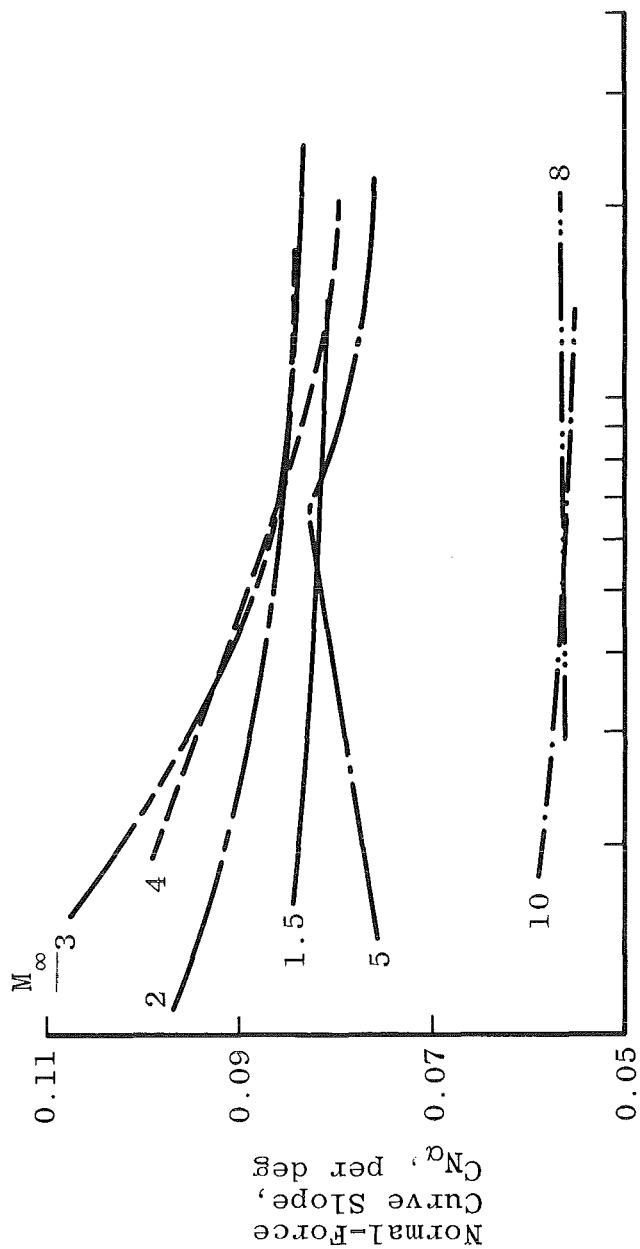
a. Configuration HB-1

Fig. 10 Mach Number Effect on Stability Parameters at Maximum Reynolds Number



b. Configuration HB-2

Fig. 10 Concluded



b. Configuration HB-2

Fig. 11 Concluded

FORCE TESTS OF STANDARD HYPERVELOCITY
BALLISTIC MODELS HB-1 AND HB-2
AT MACH 1.5 TO 10

By
J. Don Gray and E. Earl Lindsay
von Kármán Gas Dynamics Facility
ARO, Inc.
a subsidiary of Sverdrup and Parcel, Inc.

August 1963

ARO Project No. VT2116

ABSTRACT


The aerodynamic characteristics of two standard, hypervelocity, ballistic-type models, designated HB-1 and HB-2, have been investigated in the supersonic and hypersonic regimes in the von Kármán Gas Dynamics Facility tunnels. The tests were conducted at nominal Mach numbers of 1.5, 2, 3, 4, 5, 8, and 10 at Reynolds numbers from 0.07 to 2.55×10^6 , based on body diameter, and through an angle-of-attack range from -2 to 15 deg. The effects of Mach number, Reynolds number, and model attitude on the static stability and axial-force characteristics of the two configurations were investigated. The zero-lift, forebody, axial-force coefficient, C_A , for both configurations was found to be sensitive to Reynolds number variations; whereas the initial normal-force curve slope, C_{N_α} , and center-of-pressure, x_{cp}/ℓ , for only the flared-tail model (HB-2) were dependent upon the Reynolds number.

PUBLICATION REVIEW

This report has been reviewed and publication is approved.



Darreld K. Calkins
Major, USAF
AF Representative, VKF
DCS/Test



Jean A. Jack
Colonel, USAF
DCS/Test

CONTENTS

	<u>Page</u>
ABSTRACT	iii
NOMENCLATURE	vii
1.0 INTRODUCTION	1
2.0 APPARATUS	
2.1 Wind Tunnels	1
2.2 Models	2
2.3 Instrumentation and Measurement Uncertainty . .	2
3.0 RESULTS AND DISCUSSION.	3
3.1 Axial-Force Characteristics	3
3.2 Stability Characteristics	5
CONCLUSIONS	7
REFERENCES	7

TABLE

1. Completed Force Test Program Summary	9
---	---

ILLUSTRATIONS

Figure

1. Wind Tunnels	
a. The 12-Inch Supersonic Tunnel (D)	11
b. The 40-Inch Supersonic Tunnel (A)	12
c. The 50-Inch Mach 8 Tunnel (B)	13
d. The 50-Inch Mach 10 Tunnel (C)	14
2. Standard Hypervelocity Ballistic Correlation	
Configurations	15
3. Model Photographs	16
4. Variation of Forebody Axial Force with Angle of Attack	
a. Configuration HB-1	17
b. Configuration HB-2	18
5. Effect of Mach Number on Pressure Drag and Forebody Axial Force, $\alpha = 0$	19
6. Mach Number Effect on Base Drag, $\alpha = 0$	20

<u>Figure</u>	<u>Page</u>
7. Reynolds Number Effect on Forebody Axial Force, $\alpha = 0$	
a. Configuration HB-1	21
b. Configuration HB-2	22
8. Variation of Normal-Force Characteristics with Angle of Attack at Various Mach Numbers	
a. Configuration HB-1	23
b. Configuration HB-2	24
9. Variation of Pitching-Moment Characteristics with Angle of Attack at Various Mach Numbers	
a. Configuration HB-1	25
b. Configuration HB-2	26
10. Mach Number Effect on Stability Parameters at Maximum Reynolds Number	
a. Configuration HB-1	27
b. Configuration HB-2	28
11. Reynolds Number Effect on Stability Parameters	
a. Configuration HB-1	29
b. Configuration HB-2	30
12. Schlieren Photographs of HB-2 at Supersonic Speeds (d = 1.25 in.)	
a. $M_\infty = 1.5$ and 2	31
b. $M_\infty = 3, 4,$ and 5	32

NOMENCLATURE

A	Reference area, $\frac{\pi d^2}{4}$, in. ²
A_b	Base area, in. ²
C_A	Forebody axial-force coefficient, $(C_{A_t} - C_{A_b})$
C_{A_b}	Base axial-force coefficient, $-C_{p_b}(A_b/A)$
C_{A_t}	Total axial-force coefficient, $\frac{\text{total axial force}}{q_\infty A}$
C_m	Pitching-moment coefficient, pitching moment/ $q_\infty A d$ (reference point 1.950d from nose)
C_N	Normal-force coefficient, normal force/ $q_\infty A$
C_{N_α}	Slope of normal-force curve, $(dC_N/d\alpha)_\alpha = 0$
C_{p_b}	Base pressure coefficient, $(p_b - p_\infty)/q_\infty$
d	Reference centerbody diameter, in.
ℓ	Overall length (4.90d), in.
M_∞	Free-stream Mach number
p_b	Base pressure, psia
p_∞	Free-stream pressure, psia
q_∞	Free-stream dynamic pressure, psia
Re_d	Reynolds number, based on centerbody diameter
x_{cp}	Center of pressure, in.
α	Angle of attack, deg

1.0 INTRODUCTION

Force tests have been conducted on two standard, hypervelocity, ballistic-type models, designated as HB-1 (blunt-nose cylinder configuration) and HB-2 (same as HB-1 with a flared afterbody), in the supersonic and hypersonic wind tunnels of the von Kármán Gas Dynamics Facility (VKF), Arnold Engineering Development Center (AEDC), Air Force Systems Command (AFSC). These models were designed in accordance with specifications originally suggested by the VKF in 1959. The purpose of designing and testing these models was to extend the speed range for correlation of wind tunnel data, after the manner adopted by the AGARD many years ago for the transonic and supersonic regimes.

Representative results of the force tests are presented for configurations HB-1 and HB-2 at nominal Mach numbers of 1.5, 2, 3, 4, and 5 in the 12- and 40-in. supersonic tunnels and at Mach 8 and 10 in the 50-in. tunnels of the VKF. The tests were conducted at several Reynolds numbers at each Mach number and with stagnation temperatures sufficient to prevent liquefaction of the tunnel air. A summary of the completed test program for HB-1 and HB-2 is presented in Table 1.

2.0 APPARATUS

2.1 WIND TUNNELS

The 12-Inch Supersonic Tunnel (D) (Fig. 1a) is an intermittent, variable density wind tunnel with a manually adjusted, flexible plate-type nozzle. The tunnel operates at Mach numbers from 1.5 to 5 at stagnation pressures from about 5 to 60 psia and at stagnation temperatures up to about 100°F.

The 40-in. supersonic and 50-in. hypersonic tunnels are continuous, closed circuit, variable density wind tunnels.

The 40-Inch Supersonic Tunnel (A) (Fig. 1b) has a flexible plate-type nozzle which is automatically driven to produce Mach numbers from 1.5 to 6. The tunnel operates at maximum stagnation pressures

Manuscript received May 1963.

from 29 to 200 psia at $M_\infty = 1.5$ to 6, respectively, and at stagnation temperatures up to 300°F ($M_\infty = 6$). Minimum operating pressures are about one-tenth of the maximum.

The 50-Inch Mach 8 Tunnel (B) (Fig. 1c) has a contoured axisymmetric nozzle and operates at stagnation pressures from 100 to 900 psia. A propane-fired combustion heater is used to provide stagnation temperatures up to about 900°F.

The 50-Inch Mach 10 Tunnel (C) (Fig. 1d) has a contoured axisymmetric nozzle and may be operated at stagnation pressures from 175 to about 2000 psia. The combustion heater along with an electric heater are utilized to produce stagnation temperatures to about 1450°F.

A more complete description of the tunnels and airflow calibration information may be found in Ref. 1.

2.2 MODELS

Geometric details of the two configurations, HB-1 and HB-2, are presented in Fig. 2 and photographs are shown in Fig. 3. As may be observed, the distinction between configurations is in the flared afterbody on HB-2. Three different size models were fabricated for each configuration with the diameters chosen to yield the maximum size consistent with blockage and shock-reflection considerations for the four wind tunnels previously described. The 1.25-in. -diam models were designed for the 12-in. supersonic tunnel. The 4.00-in. -diam models were designed for the 40-in. supersonic tunnel and the 7.50-in. -diam models for the 50-in. hypersonic tunnels. All of the models were fabricated of stainless steel. The surface finish of all models was of the order of 16 rms microinches. All models were supported by cylindrical stings. The stings for the 1.25-in. models were 3/4-in. and 1-in. diam by approximately 8-in. long. The larger models were supported by stings whose diameters were equal to or less than $0.3d$ and whose lengths were equal to or greater than $3.0d$.

2.3 INSTRUMENTATION AND MEASUREMENT UNCERTAINTY

Normal force, pitching moment, and axial force were measured with six-component, internal strain-gage, moment-type balances. Because of the extreme range of loads involved, six balances were used. The force capacities of each balance and the corresponding statistical uncertainties (σ) of measurement are provided by the following table:

	Supersonic				Hypersonic	
	1	2	3	4	5	6
Balance						
Normal Force F_N , lb	---	---	15	125	100	300
σF_N , lb	---	---	± 0.04	± 0.17	± 0.23	± 0.54
Axial Force F_A , lb	3	8	30	300	30	100
σF_A , lb	± 0.006	± 0.033	± 0.035	± 0.560	± 0.044	± 0.440
Pitching Moment M_Y , in. -lb	---	---	66	625	400	1750
σM_Y , in. -lb	---	---	± 0.06	± 1.59	± 0.29	± 1.36

Base pressures, for correction of the axial force, were measured by 1- and 5-psid transducers referenced to a near vacuum. The precision of measurement is considered to be about ± 0.005 - and ± 0.025 -psia, respectively, for the two transducer ratings. The base pressures were measured in the model cavity and were assumed to represent the pressure acting over the entire base area of the model.

3.0 RESULTS AND DISCUSSION

The aerodynamic characteristics for configurations HB-1 and HB-2 are presented in Figs. 4 through 11. The variations of normal-force, pitching-moment, and forebody axial-force coefficients represent the results at maximum Reynolds number, based on body diameter, at each test Mach number. Additional data are presented in the form of forebody axial-force coefficient at zero lift, and the stability parameters C_{N_α} and x_{cp}/l as functions of Reynolds number and Mach number to provide additional data for correlation purposes.

3.1 AXIAL-FORCE CHARACTERISTICS

The effects of angle of attack upon the forebody axial-force coefficient at Mach numbers of 1.5 through 10 are shown by the curves in Fig. 4. Data at maximum Reynolds number are given in Fig. 4a for HB-1 and in Fig. 4b for HB-2. For both configurations, it is apparent that Mach number has a significant effect upon the

change of C_A with angle of attack. In particular, at Mach 1.5 the forebody axial-force coefficient decreased with angle of attack, whereas at Mach numbers greater than 3.0, C_A increased with angle of attack for both HB-1 and HB-2.

The variation of the zero-lift, forebody axial-force coefficient with Mach number for HB-1 and HB-2 is shown in Fig. 5 for the case of maximum free-stream Reynolds number. The wave or pressure drag variation of the two configurations is included to verify the trends and to illustrate the small contribution of skin friction to the forebody axial-force coefficient at maximum Reynolds number. The convergence of results for the two configurations as the Mach number increased is evidence that the wave drag contribution of the flare decreased significantly with Mach number. The rise in drag of both shapes at Mach 10 relative to Mach 8 is interpreted as a viscous drag increase.

The base drag contributions under the same conditions are presented in Fig. 6, and it is to be noted that the base-drag coefficient smoothly decreases to near zero for HB-2 and to slightly negative (thrust) values for HB-1 at hypersonic speeds.

The effects of free-stream Reynolds number variation on the zero-lift forebody axial-force coefficient are shown in Fig. 7. Since there is no boundary-layer separation on HB-1 and because the wave drag of the nose (HB-1) would be insensitive to Reynolds number in the range under consideration, the effects shown in Fig. 7a may be interpreted as caused by skin-friction drag only. It may be seen that data for different scale models correlate well. At Mach numbers of 2 and greater, the trend of increasing sensitivity of C_A to Reynolds number is particular evidence of the reduction in local Reynolds number caused by the bow-wave entropy rise as free-stream Mach number is increased.

The axial-force variation for the flared tail configuration, HB-2, is shown in Fig. 7b. In the supersonic range the functional dependence of C_A upon Reynolds number is markedly different from that for HB-1. The primary reason for this is due to the occurrence of laminar boundary layer separation ahead of the flare, the extent of which decreases with increasing Reynolds number. Thus, the trends shown near maximum Reynolds number at $M_\infty \leq 5$ are primarily due to wave-drag increases for the flare. When C_A levels off, as at Mach 1.5, 2, and 3, the laminar separation had either disappeared or was decreased to an extent that may be considered effectively absent. A different effect of Reynolds number is evident at $4 \leq M_\infty \leq 5$ wherein a minimum axial-force coefficient is reached at intermediate Re_d . The cause of

this is unresolved by schlieren photographs, but the photographs do indicate that re-attachment is upstream of the flare rim in the Reynolds number range below this Re_d for minimum C_A . If the extent of separation did not change appreciably, this drag rise could be explained by the skin friction rise shown for HB-1. However, if the separation region increased, the skin friction contribution would be expected to decline, in which case the increase shown could only be caused by a pressure-drag rise. Pressure distribution results are required to resolve this interesting situation.

3.2 STABILITY CHARACTERISTICS

The effect of Mach number upon the variation of normal-force coefficient with angle of attack at maximum Reynolds number is presented in Fig. 8a for HB-1 and Fig. 8b for HB-2. In general, the variation of C_N is essentially linear with α for both configurations at these Reynolds and Mach numbers for angles below about 6 deg.

Pitching-moment coefficient versus angle of attack is shown in Fig. 9 over the Mach number range at angles of attack to about 14 deg. Configuration HB-1 is, in general, unstable about the chosen reference (Fig. 9a); however, at different angles, depending upon the Mach number, the rate-of-change of C_m with α becomes highly non-linear. The addition of the flared tail (HB-2) is shown in Fig. 9b to produce stabilizing moments at all Mach numbers over the full angle-of-attack range. Pronounced non-linearities in the curves at Mach 4 and 5 are evident for angles less than 6 deg. Such behaviour at small angles of attack is characteristic of the differential movement of boundary-layer reattachment around the flare circumference.

The effects of Mach number upon stability parameters C_{N_α} and x_{cp}/ℓ are presented in Fig. 10a for HB-1 where it is shown that a peak value of C_{N_α} was reached between Mach 2 and 3, whereas the most aft position of center of pressure, x_{cp}/ℓ , occurred near Mach 4. Modified Newtonian theory included in the figure for C_{N_α} is noted to underestimate the experimental results even at Mach 10, but this is not unreasonable because of neglect of the cylinder lift in the analysis. For the same reasons, x_{cp}/ℓ is underestimated.

The initial slopes of the normal-force curves for the flared configuration HB-2, Fig. 10b, are practically double the values produced by HB-1. The most significant result shown for these data is the appreciable reduction of C_{N_α} between Mach 5 and 8 which is attributed

to the boundary-layer separation in the region of the body-flare junction. There is no detectable effect of Mach number on the initial normal-force slopes above Mach 8. A comparison of the experimental normal-force derivatives with the modified Newtonian theory for Mach 10 shows that the experimental results are generally higher in the supersonic range yet are significantly lower at Mach 8 and 10. This indicates that the boundary-layer separation became extensive and was not appreciably affected by small pitch perturbations at hypersonic speeds. Figure 10b also shows that the addition of the flared afterbody, HB-2, moved the effective center of pressure aft of the moment reference location at Mach numbers from 1.5 to 10. Because of the boundary-layer separation effects ahead of the flare, the center of pressure is overestimated by Newtonian theory.

The influence of Reynolds number upon the stability parameters, C_{N_α} and x_{cp}/ℓ , is presented in Fig. 11 for each Mach number investigated. As expected, there is a negligible influence of Reynolds number upon both parameters at all Mach numbers for the HB-1 configuration, as shown in Fig. 11a. The Reynolds number range shown represents data obtained from models with different body diameters as given in Table 1. No size effect is discernible on these parameters for HB-1.

The flared afterbody configuration, HB-2, exhibited considerable variation of C_{N_α} and x_{cp}/ℓ with Reynolds number for the supersonic Mach numbers, Fig. 11b. At supersonic speeds through Mach 4, it is observed that reductions in Reynolds number resulted in increased magnitudes of both the initial slope of normal-force curve and the effective center of pressure. However, at Mach 5 a reversal of this trend is observed at Reynolds numbers below about 0.7×10^6 . This behavior is similar to that observed in Ref. 2 where it is shown that the cause for the reversal is associated with the extent of boundary-layer separation relative to the flare. Apparently, the separation is so extensive at Mach 8 and 10 that the influence of Reynolds number on its extent is negligible. Thus, the level of C_{N_α} would be expected to be reduced from that observed at supersonic speeds because of the effectively smaller flare angle. As was the case for HB-1, no model size effect is evident in these data for HB-2.

Some selected schlieren photographs of HB-2, which were obtained from the 12-in. supersonic tunnel, are presented in Fig. 12. These photographs are intended to show the varying existence of boundary-layer separation at $\alpha = 0$ in the flare region throughout the supersonic regime.

CONCLUSIONS

Based upon force measurements at supersonic and hypersonic speeds, over a wide range of Reynolds numbers, with different size models of the standard ballistic configurations HB-1 and HB-2, the following findings are considered of significance:

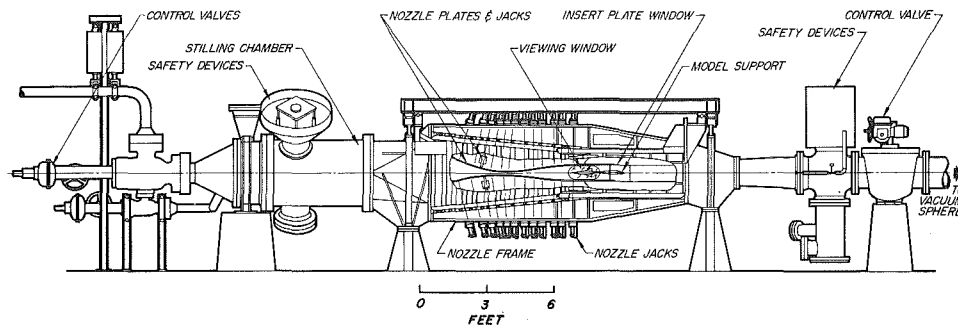
1. The forebody axial-force coefficient was found to ^{decrease} increase with angle of attack at Mach numbers less than 3 and to increase with angle of attack at all larger Mach numbers.
2. Reynolds number had a significant effect upon the zero-lift, forebody axial-force coefficient at all supersonic speeds, $M_\infty \leq 5$, for both configurations.
3. The initial slope of the normal-force curve, C_{N_α} , for both configurations was sensitive to Mach number variations below eight.
4. The effect of Reynolds number variation upon C_{N_α} , for both configurations was sensitive to Mach number variations below eight.
5. The effect of Reynolds number variation upon C_{N_α} and x_{cp}/ℓ was significant for configurations HB-2, whereas for HB-1 the influence was negligible.

REFERENCES

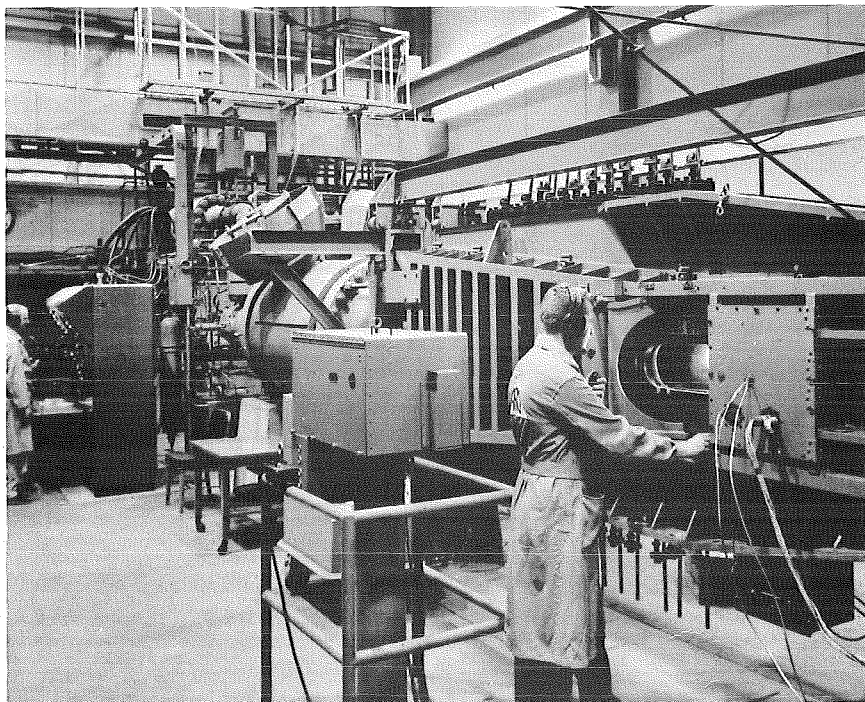
1. Test Facilities Handbook, (4th Edition). "von Kármán Gas Dynamics Facility, Vol. 4." Arnold Engineering Development Center, July, 1962.
2. Gray, J. Don. "Boundary Layer Separation Effects on the Static Stability of a Flared-Tail Missile Configuration at $M = 2$ to 5 ." AEDC TN-60-103, June 1960.

TABLE 1
COMPLETED FORCE TEST PROGRAM SUMMARY

VKF Wind Tunnel	Reynolds No. Range, $Re_d \times 10^{-6}$	Mach No. Range, M_∞	Diameter, d, in.
12 x 12 SS (D)	0.04 to 1.60	1.5 to 5.0	1.25
40 x 40 SS (A)	0.11 to 0.78	1.5 to 5.0	1.25
40 x 40 SS (A)	0.35 to 2.50	1.5 to 5.0	4.00
50-in. Mach 8 (B)	0.28 to 1.14	8.0	4.00
50-in. Mach 8 (B)	0.55 to 2.15	8.0	7.50
50-in. Mach 10 (C)	0.19 to 1.36	10	7.50

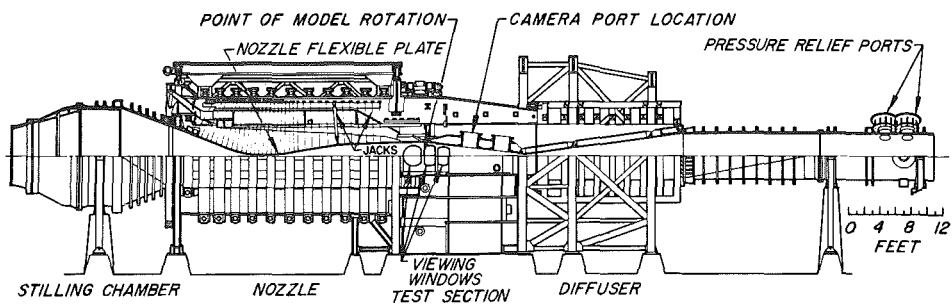


Assembly

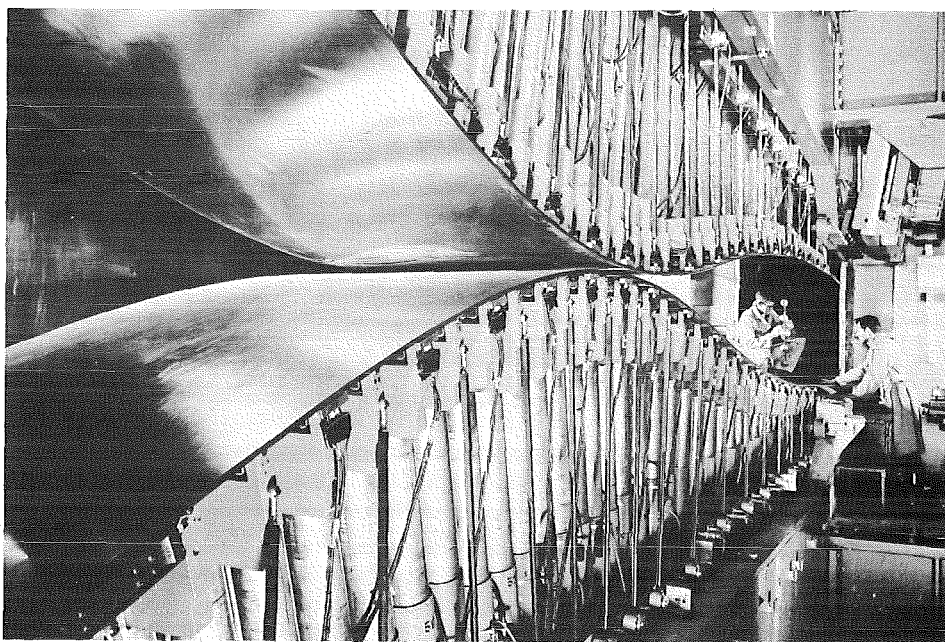


a. The 12-Inch Supersonic Tunnel (D)

Fig. 1 Wind Tunnels



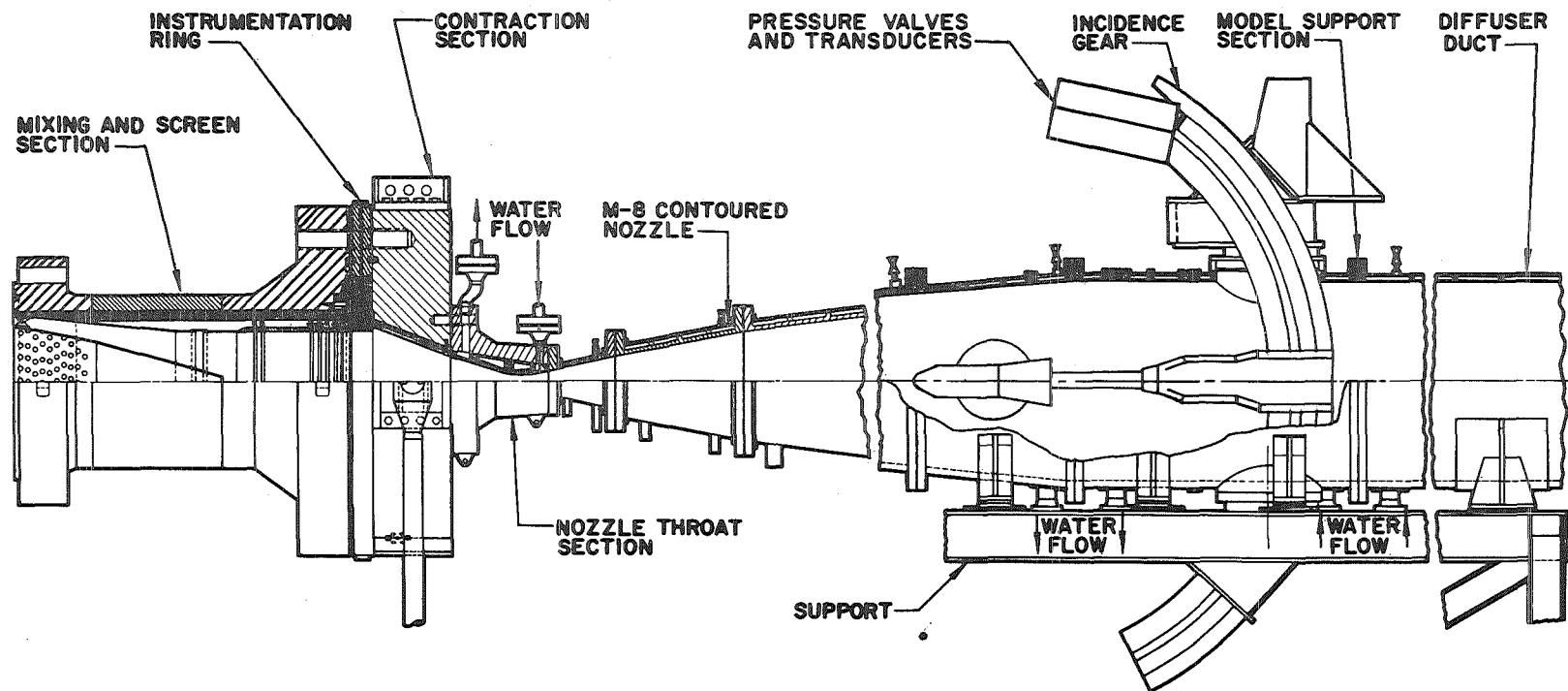
Assembly



Nozzle and Test Section

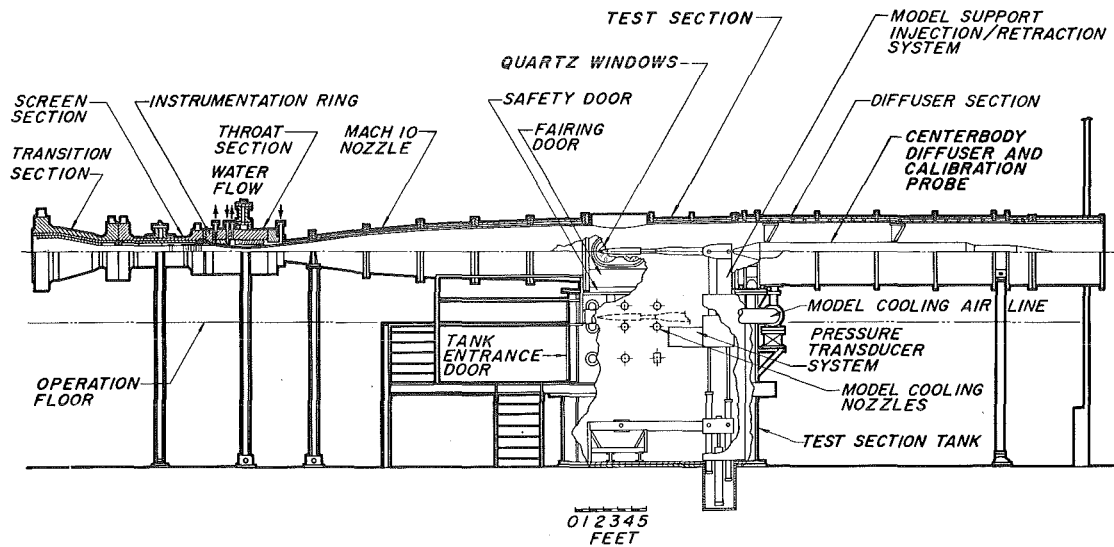
b. The 40-Inch Supersonic Tunnel (A)

Fig. 1 Continued

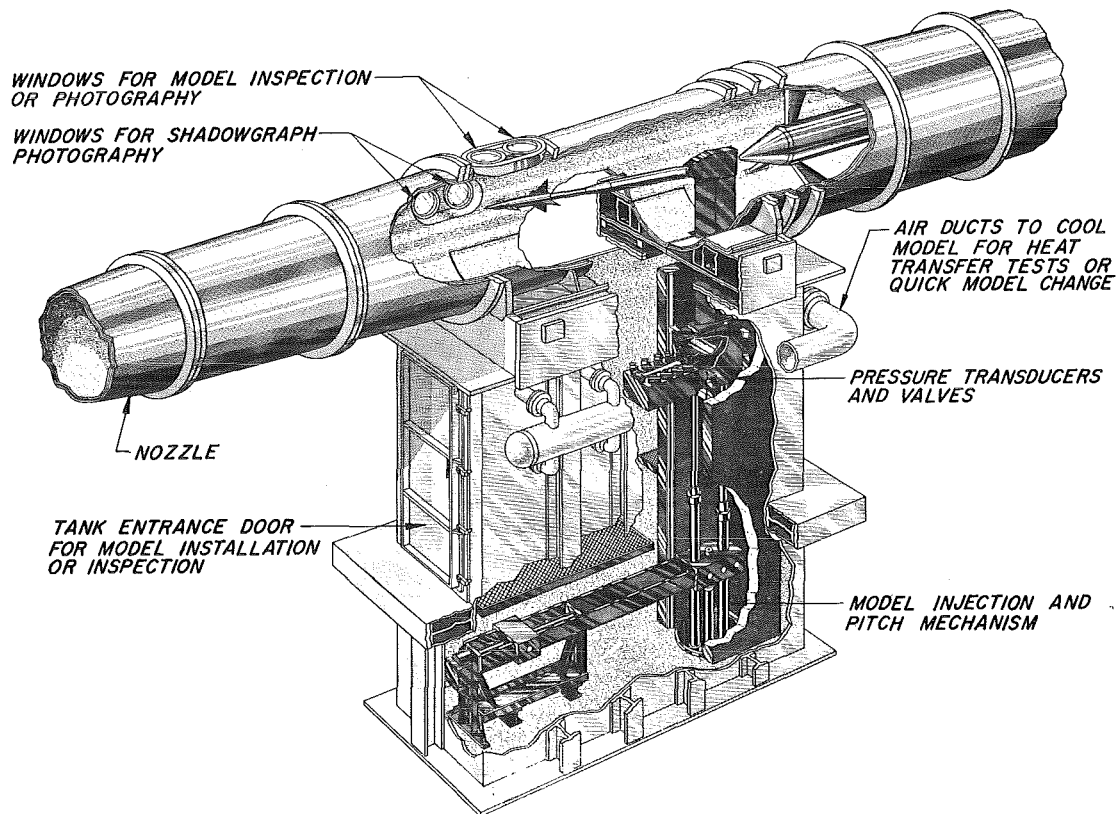


c. The 50-Inch Mach 8 Tunnel (B)

Fig. 1 Continued



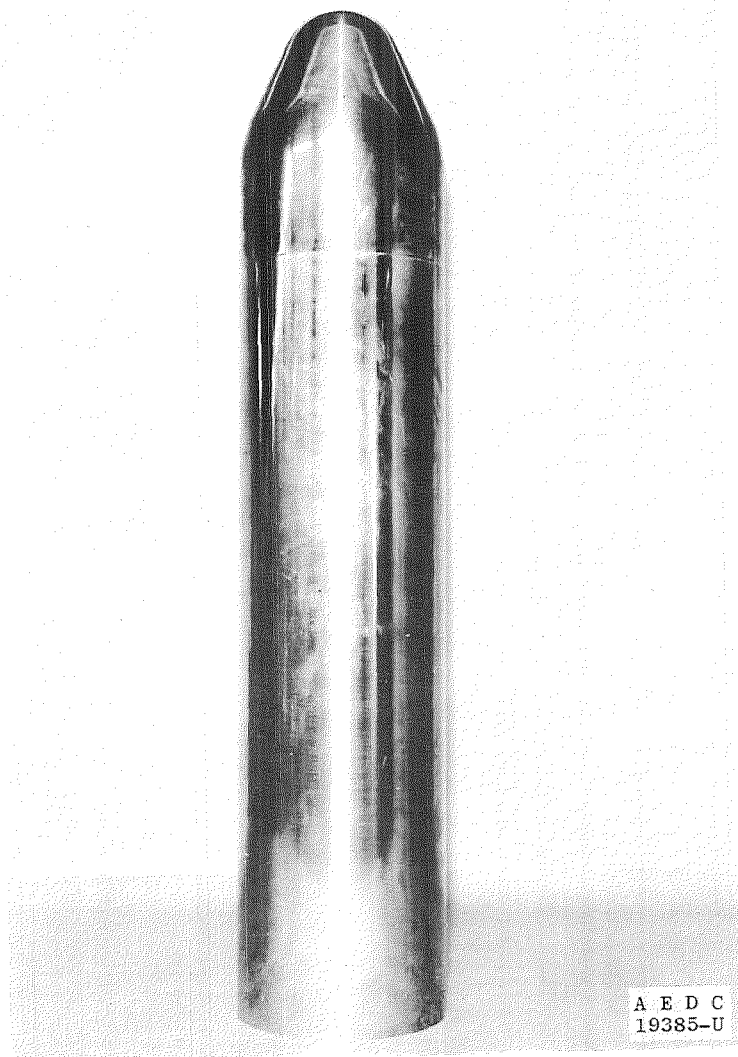
Tunnel Assembly



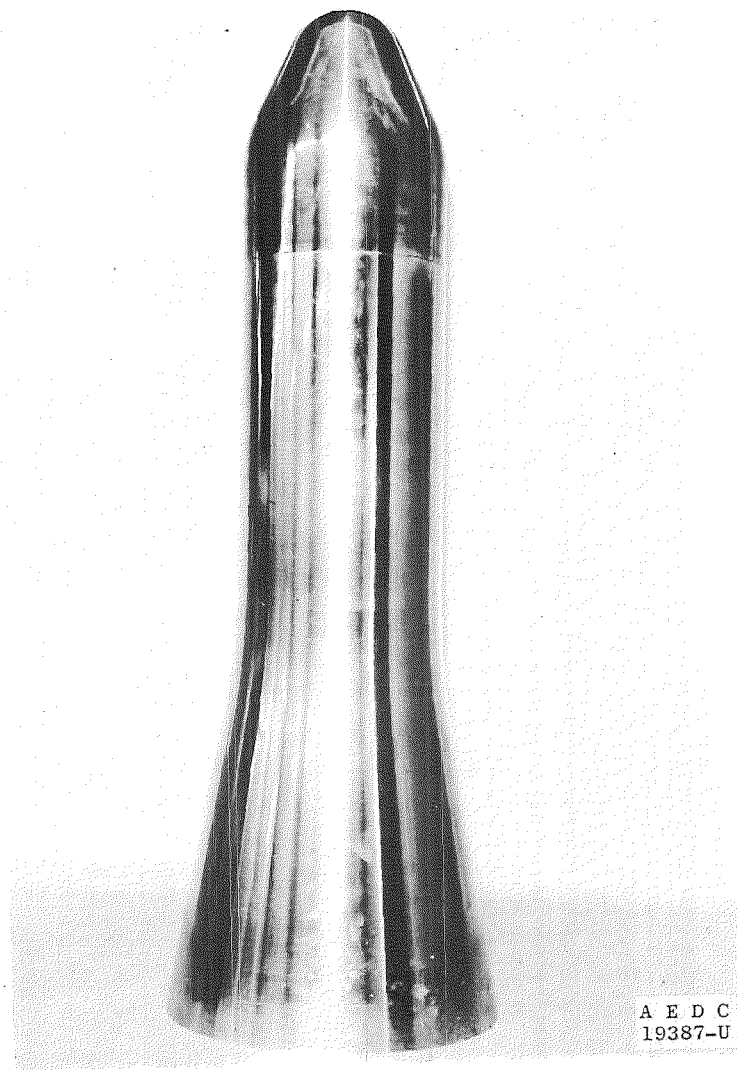
Tunnel Test Section

d. The 50-Inch Mach 10 Tunnel (C)

Fig. 1 Concluded

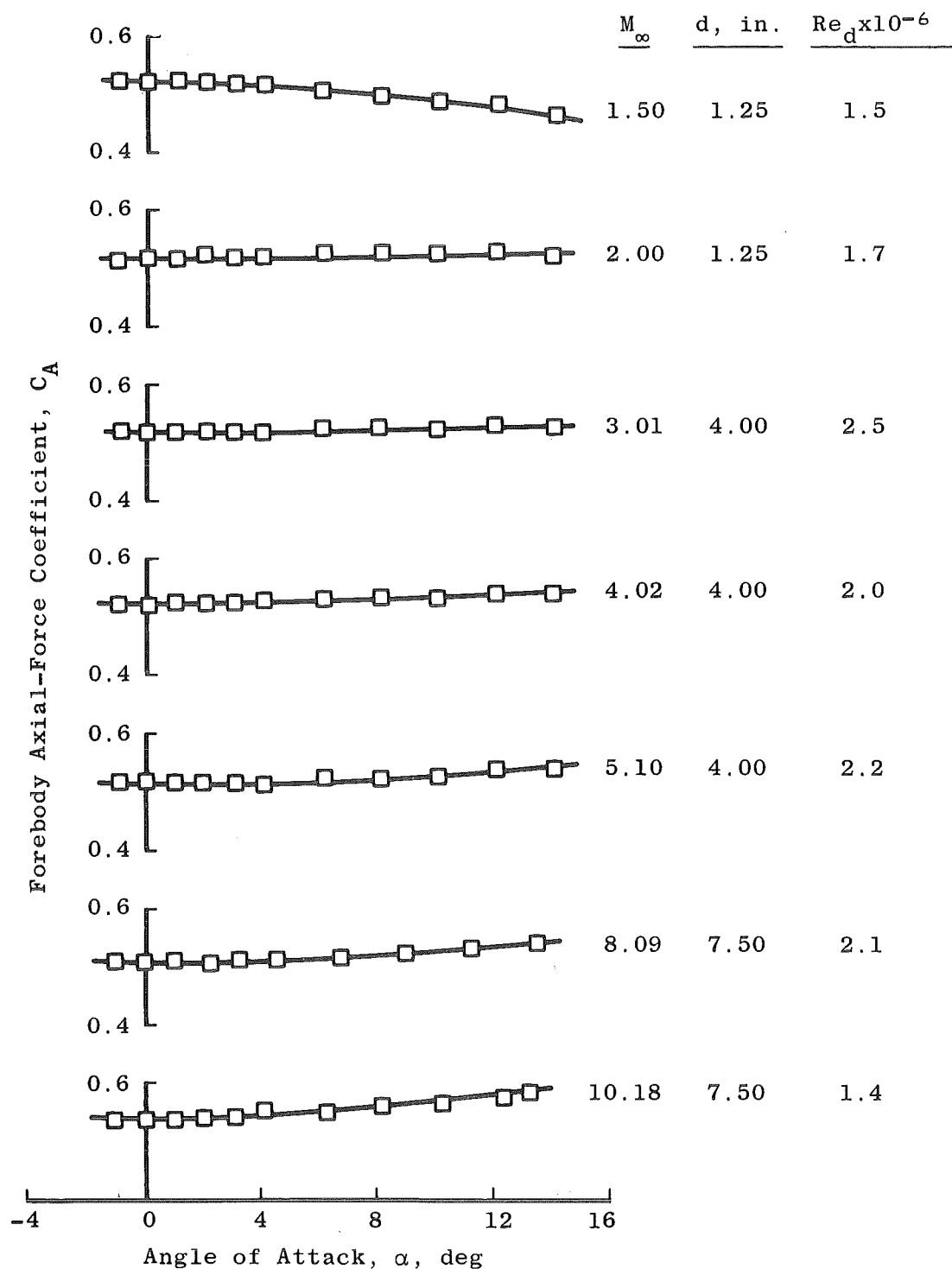


Configuration HB-1



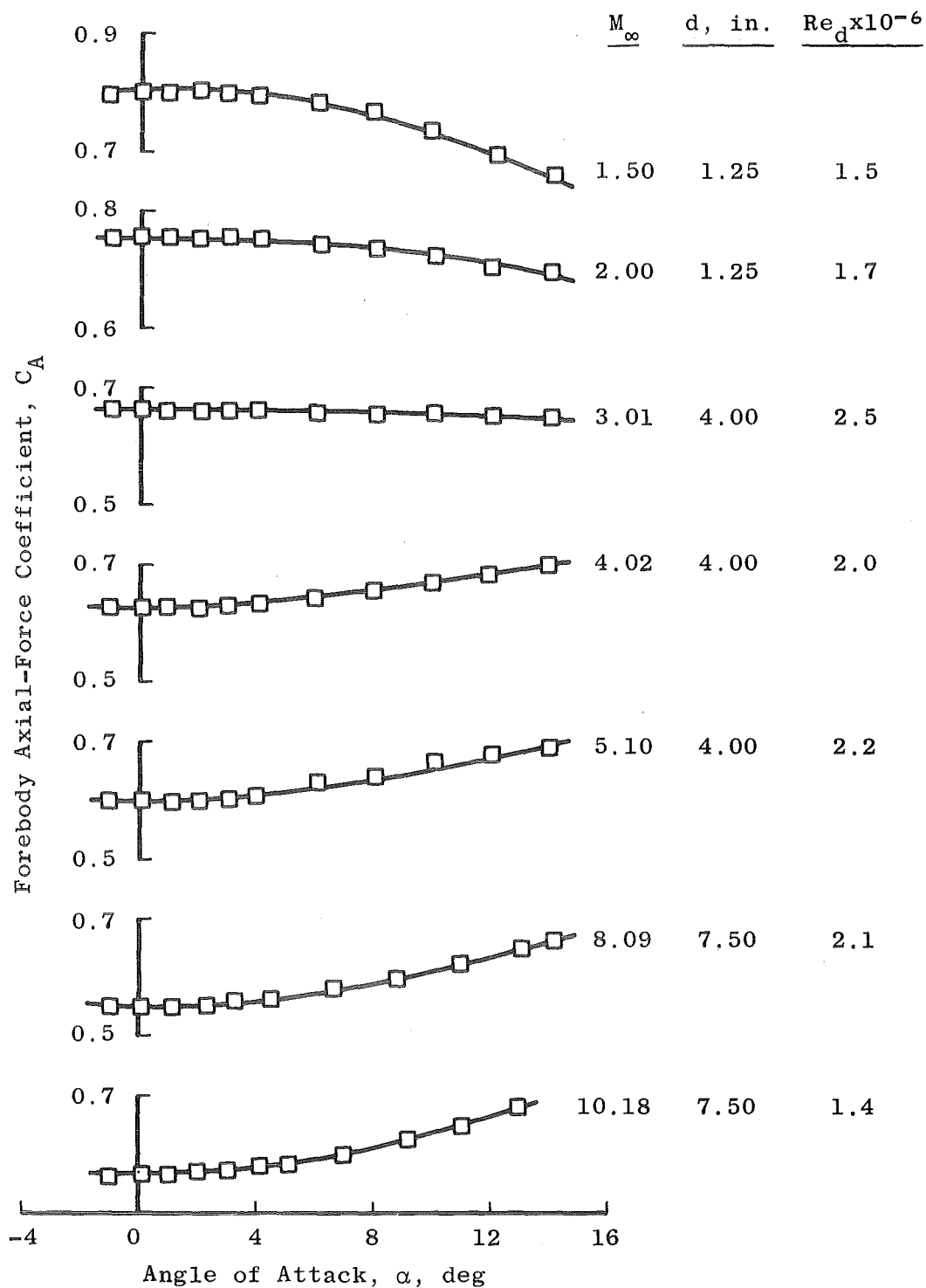
Configuration HB-2

Fig. 3 Model Photographs



a. Configuration HB-1

Fig. 4 Variation of Forebody Axial Force with Angle of Attack



b. Configuration HB-2

Fig. 4 Concluded

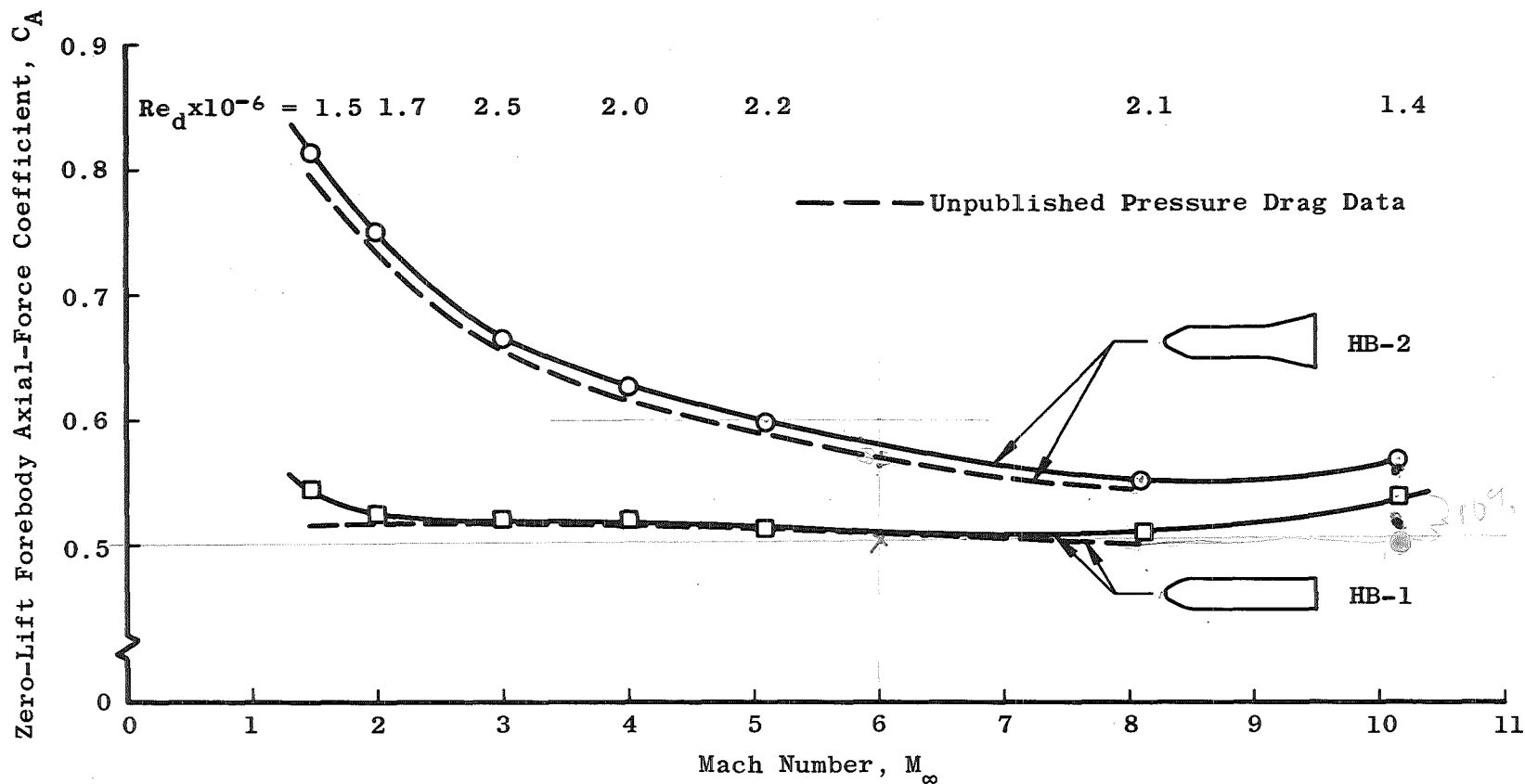


Fig. 5 Effect of Mach Number on Pressure Drag and on Forebody Axial Force, $\alpha = 0$

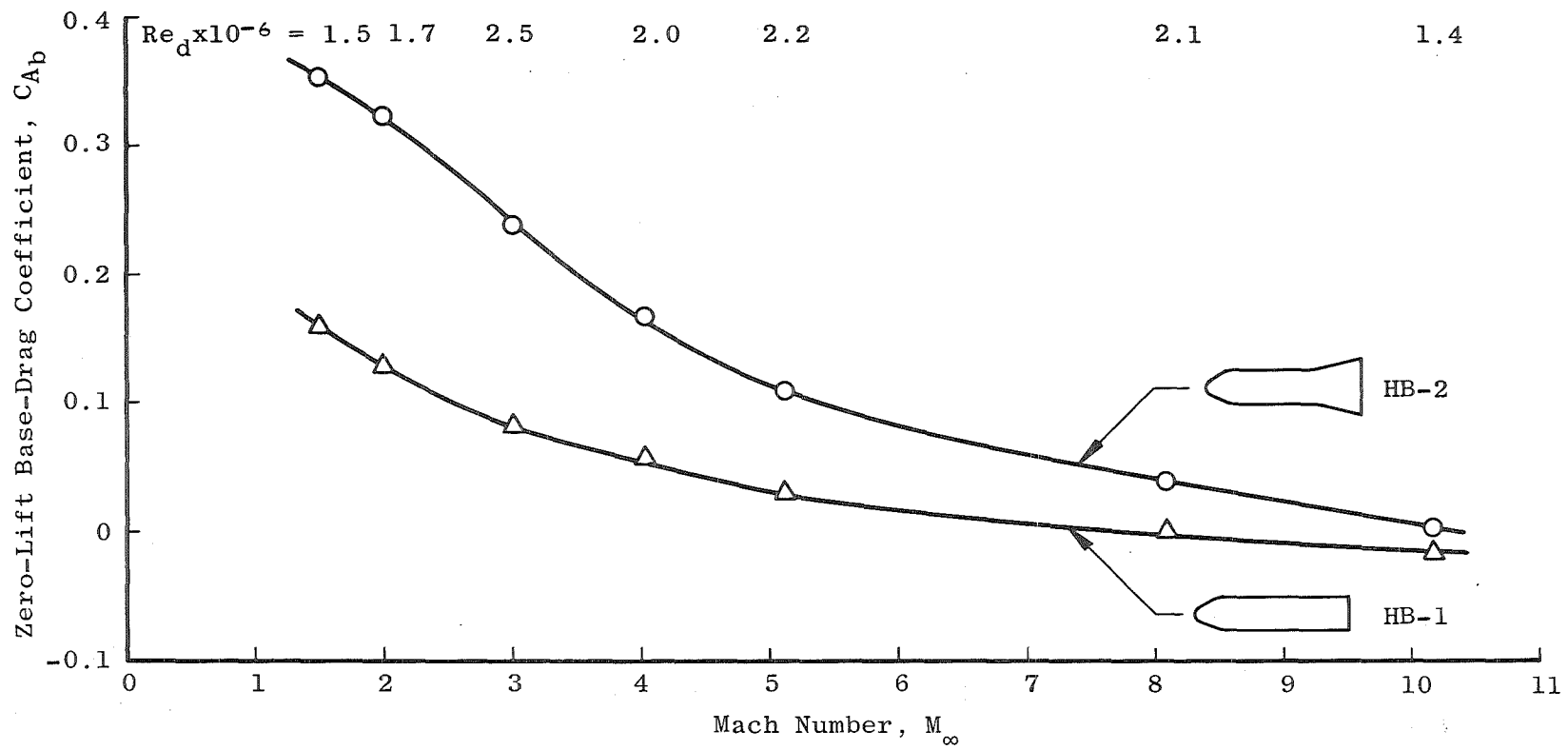
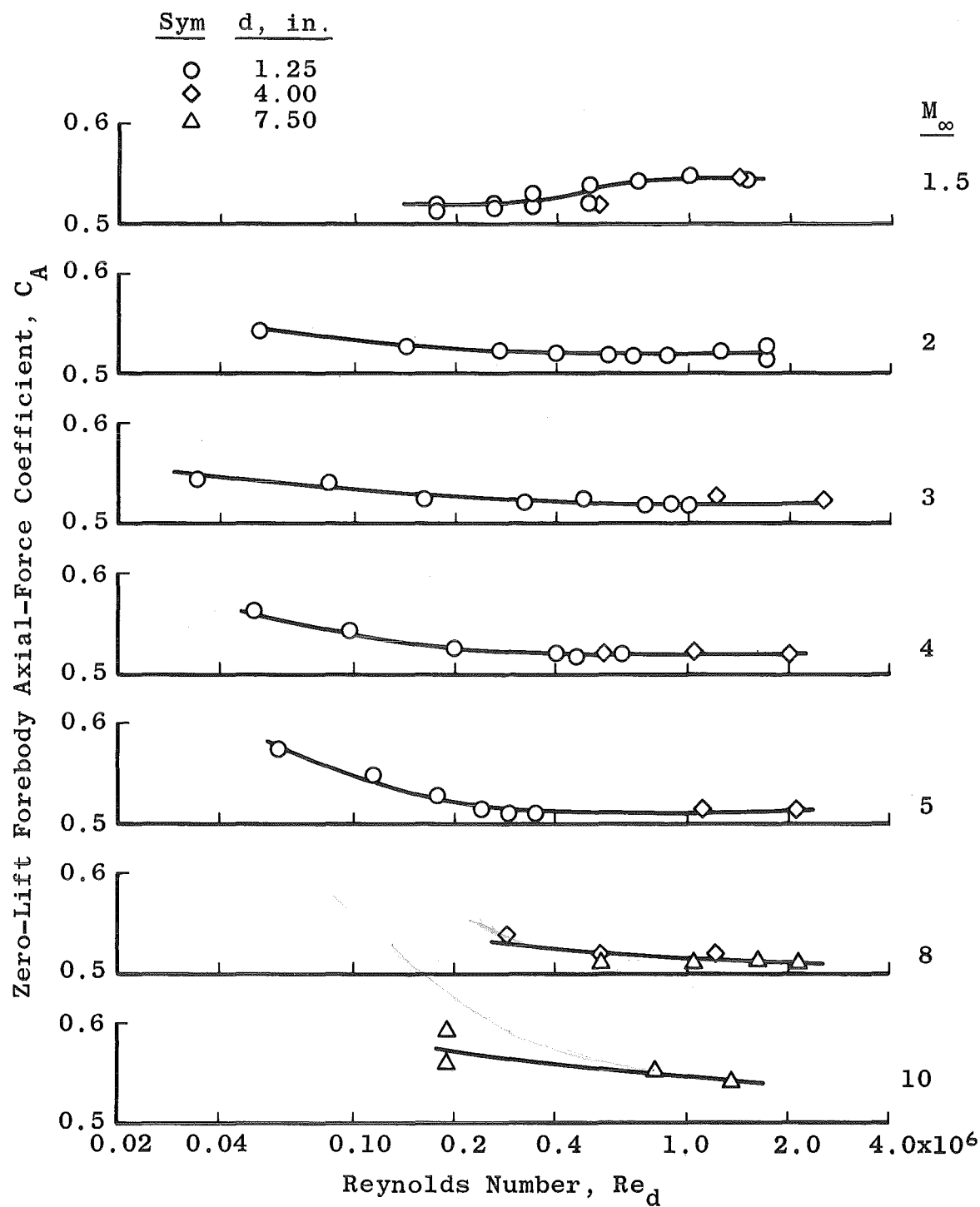
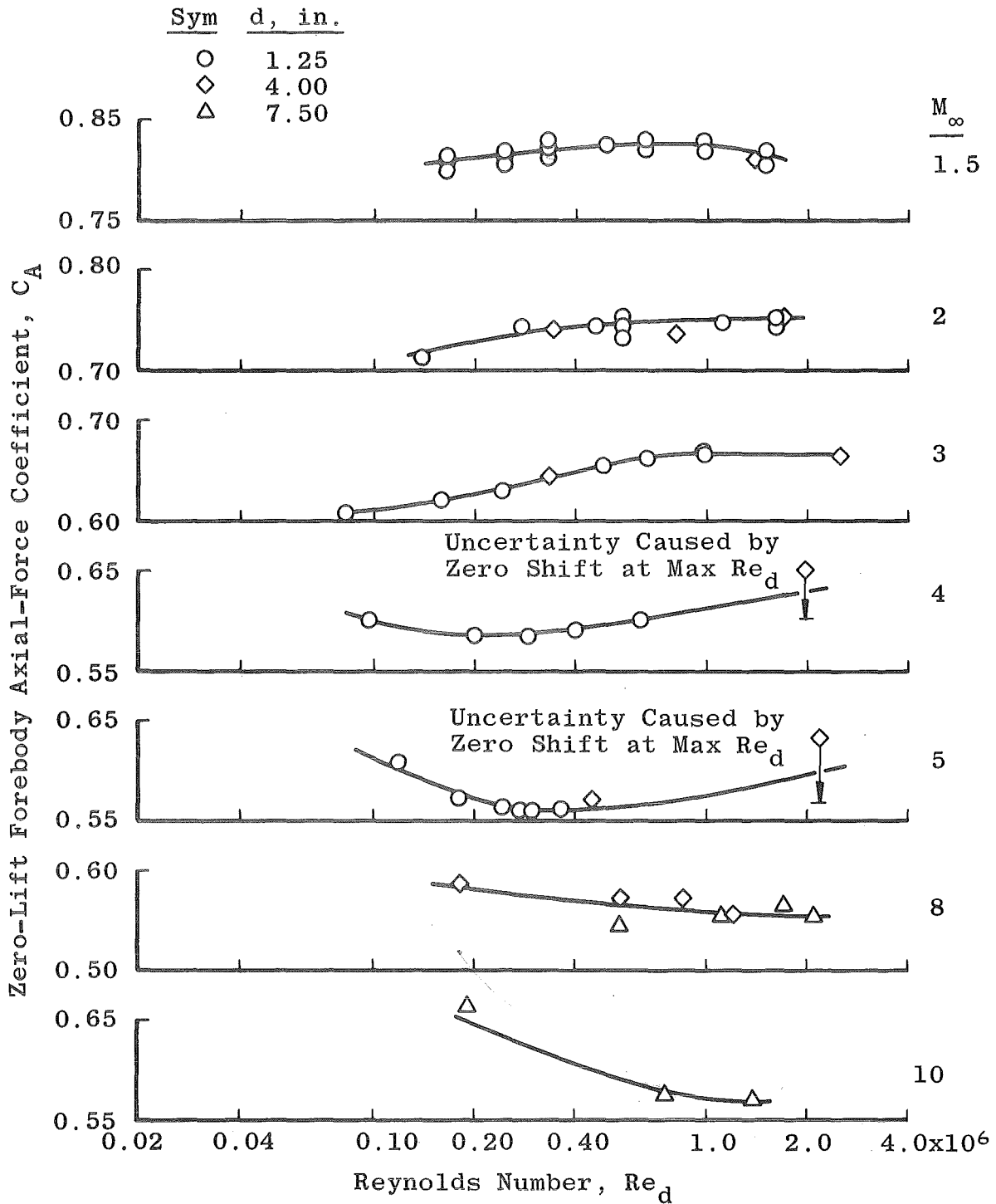


Fig. 6 Mach Number Effect on Base Drag, $\alpha = 0$



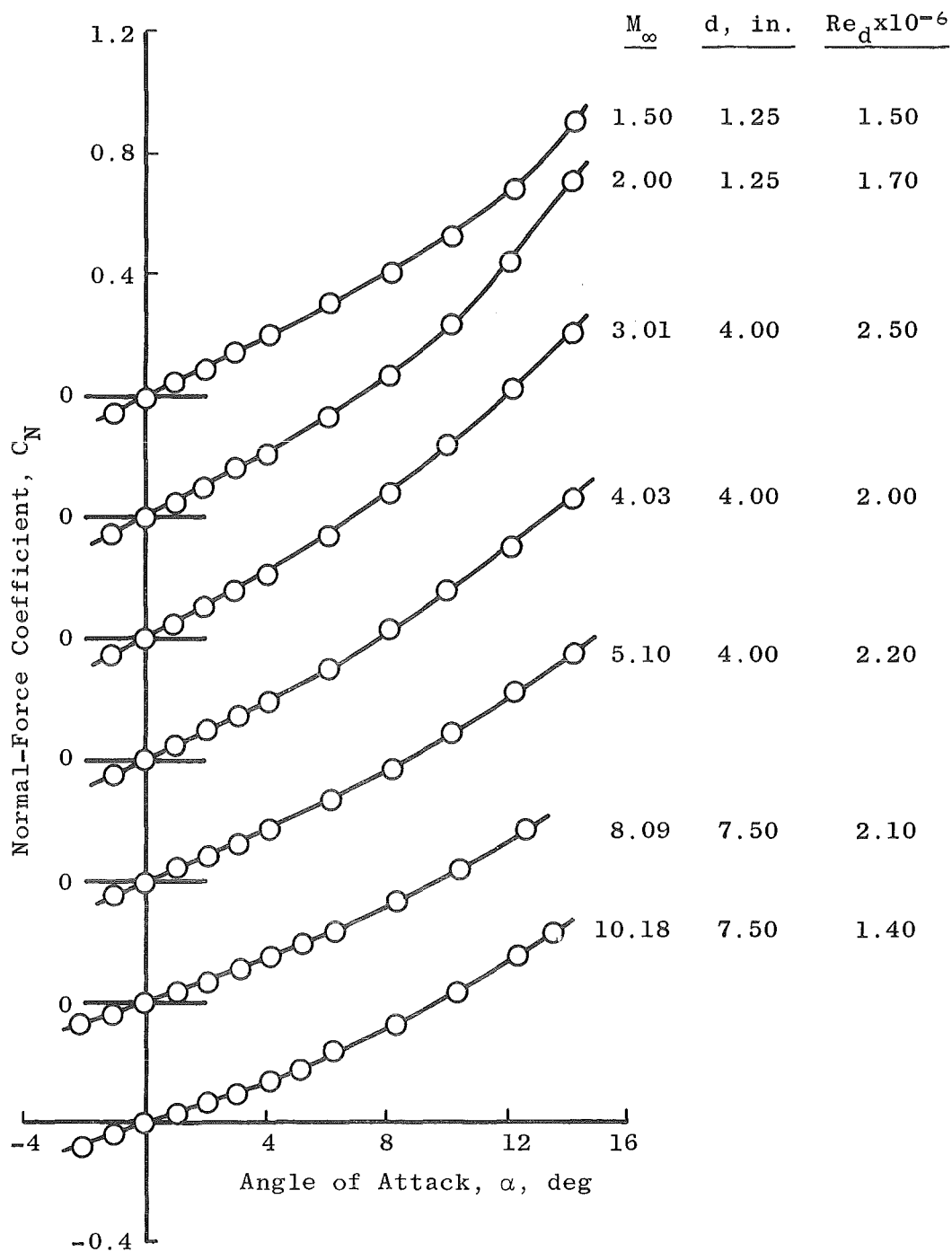
a. Configuration HB-1

Fig. 7 Reynolds Number Effect on Forebody Axial Force, $\alpha = 0$



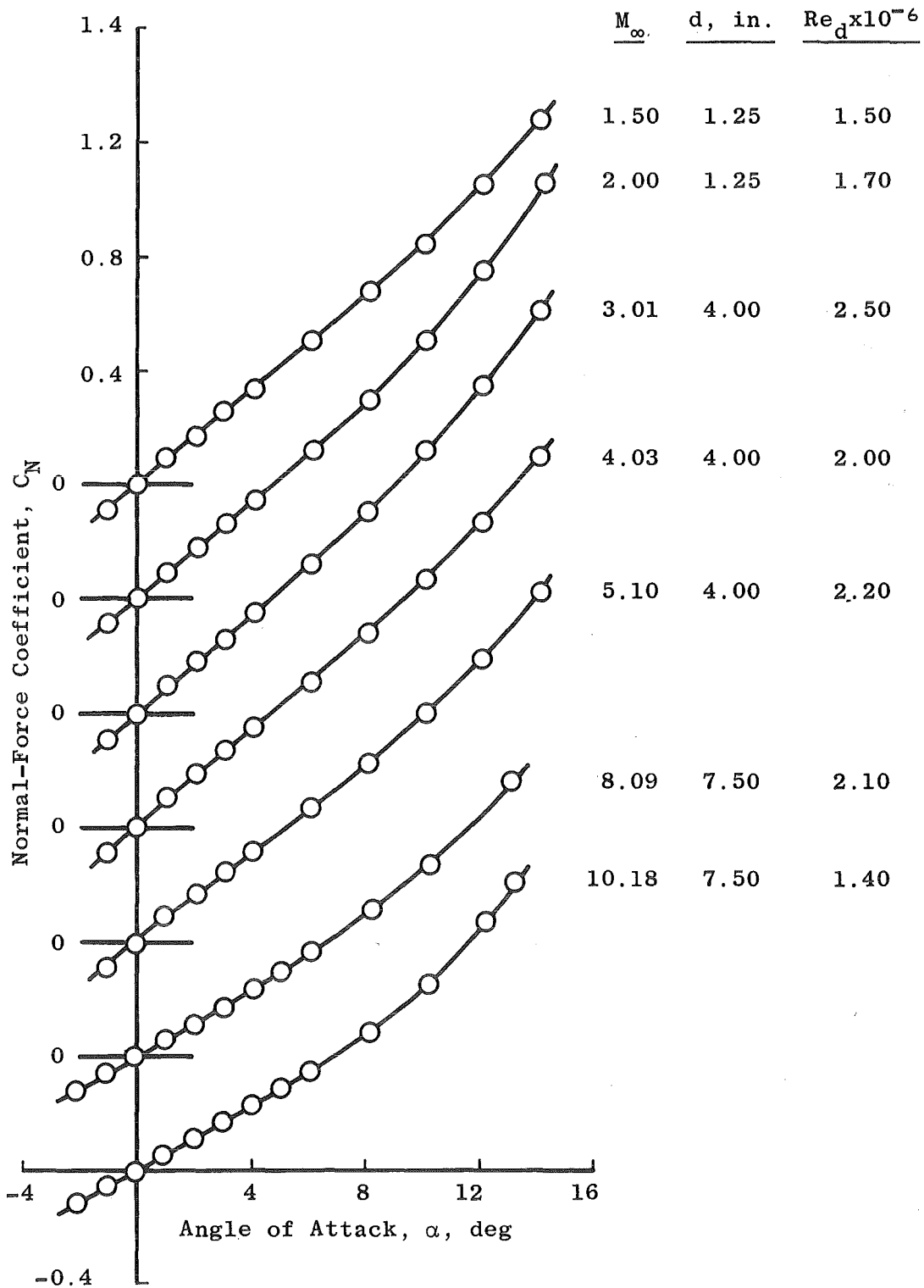
b. Configuration HB-2

Fig. 7 Concluded



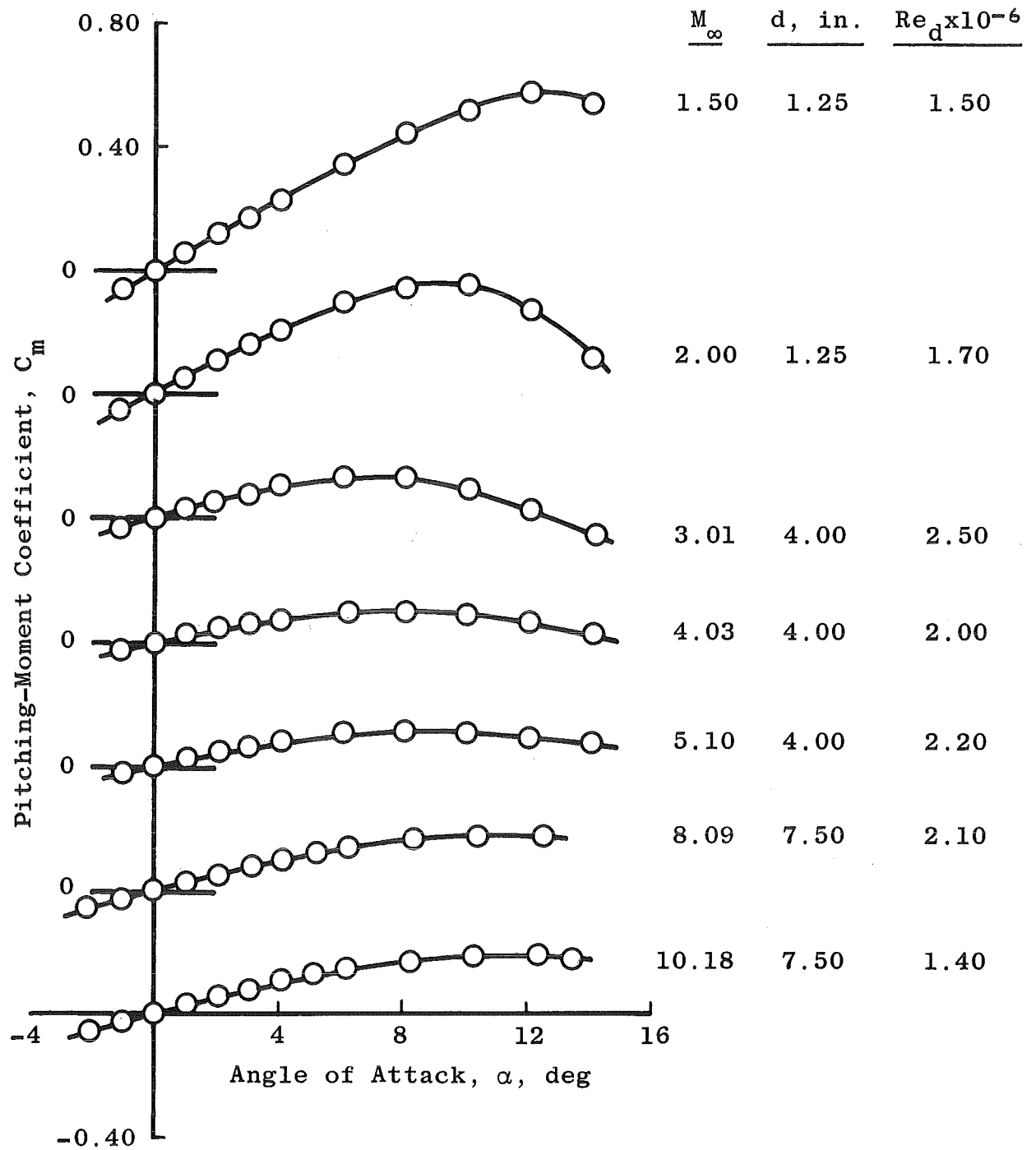
a. Configuration HB-1

Fig. 8 Variation of Normal-Force Characteristics with Angle of Attack at Various Mach Numbers



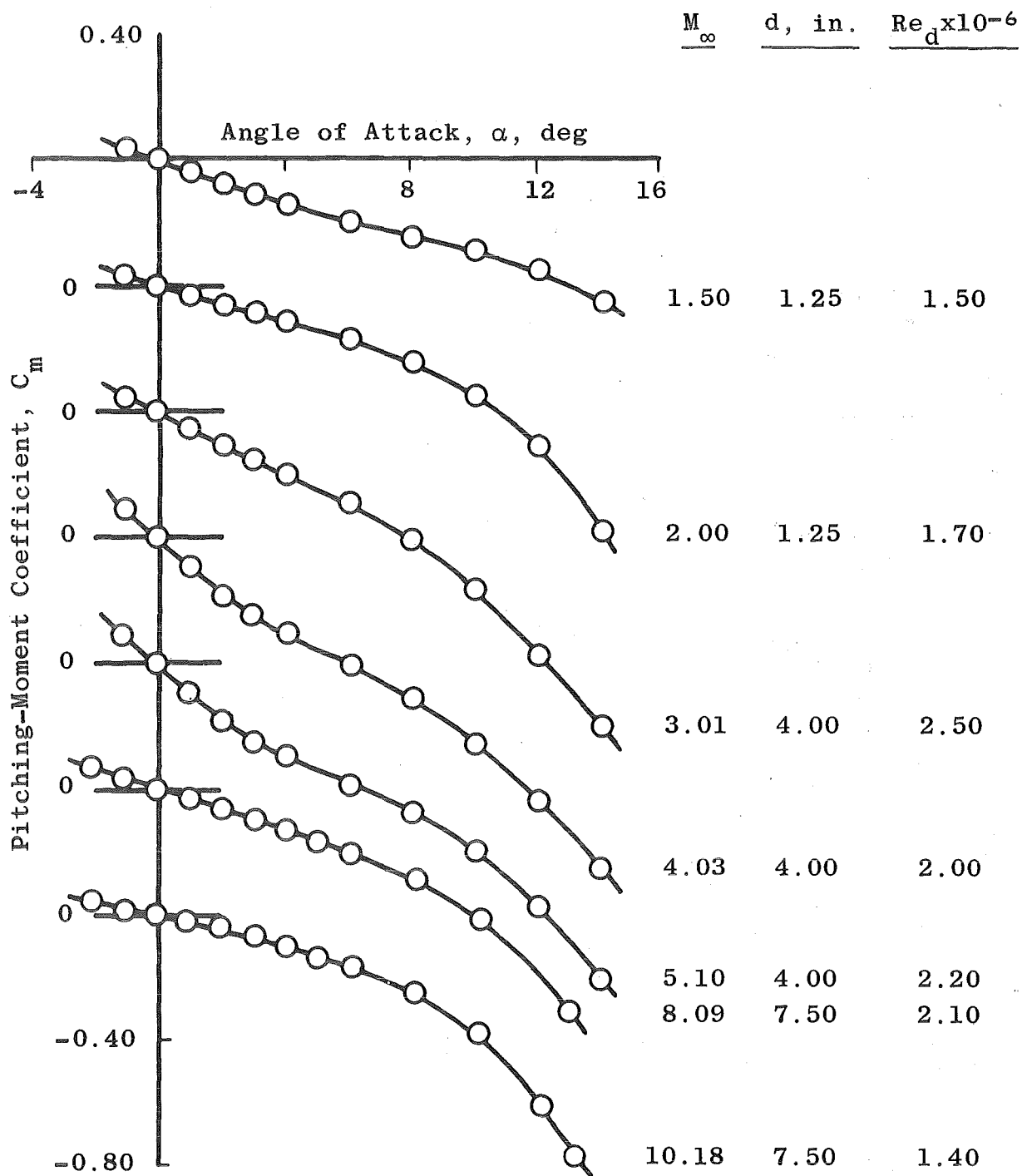
b. Configuration HB-2

Fig. 8 Concluded



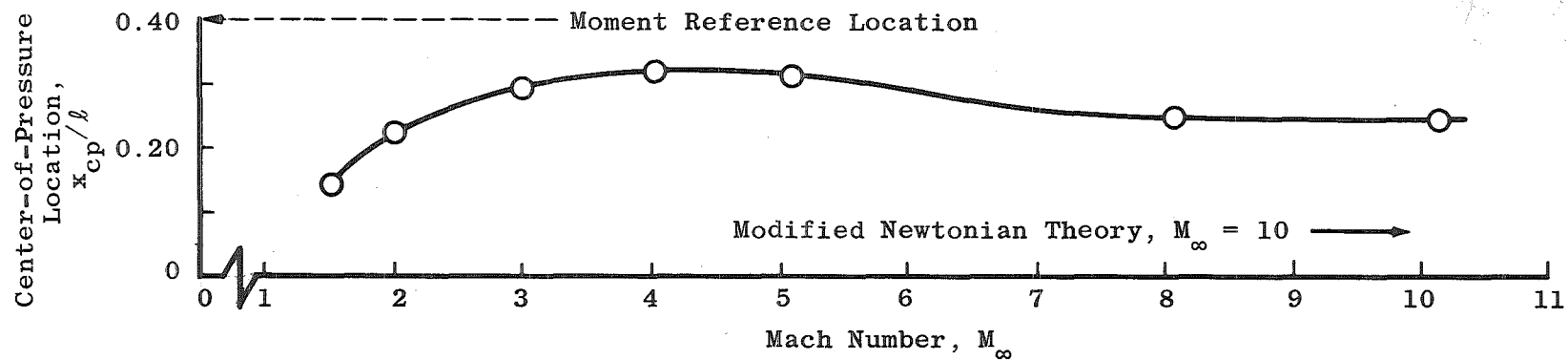
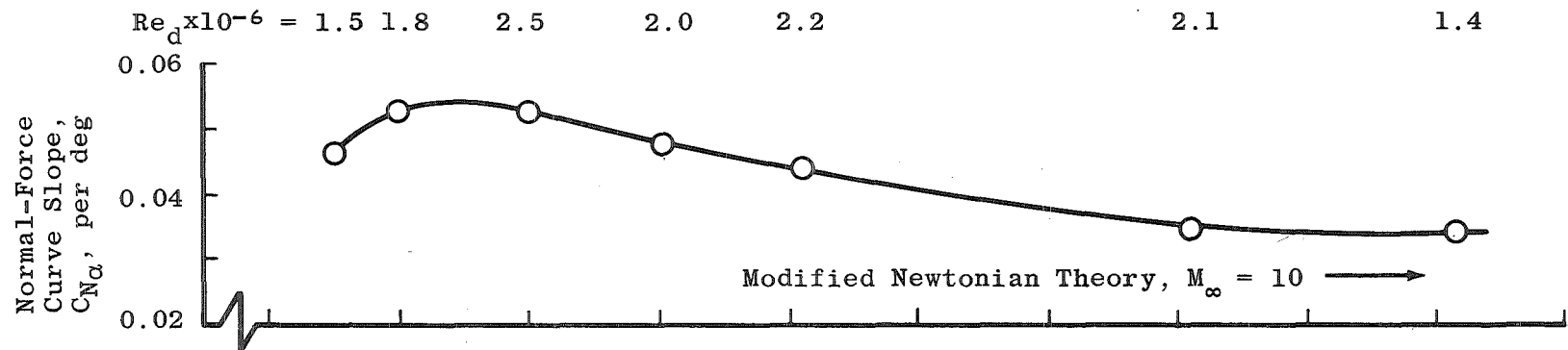
a. Configuration HB-1

Fig. 9 Variation of Pitching-Moment Characteristics with Angle of Attack at Various Mach Numbers



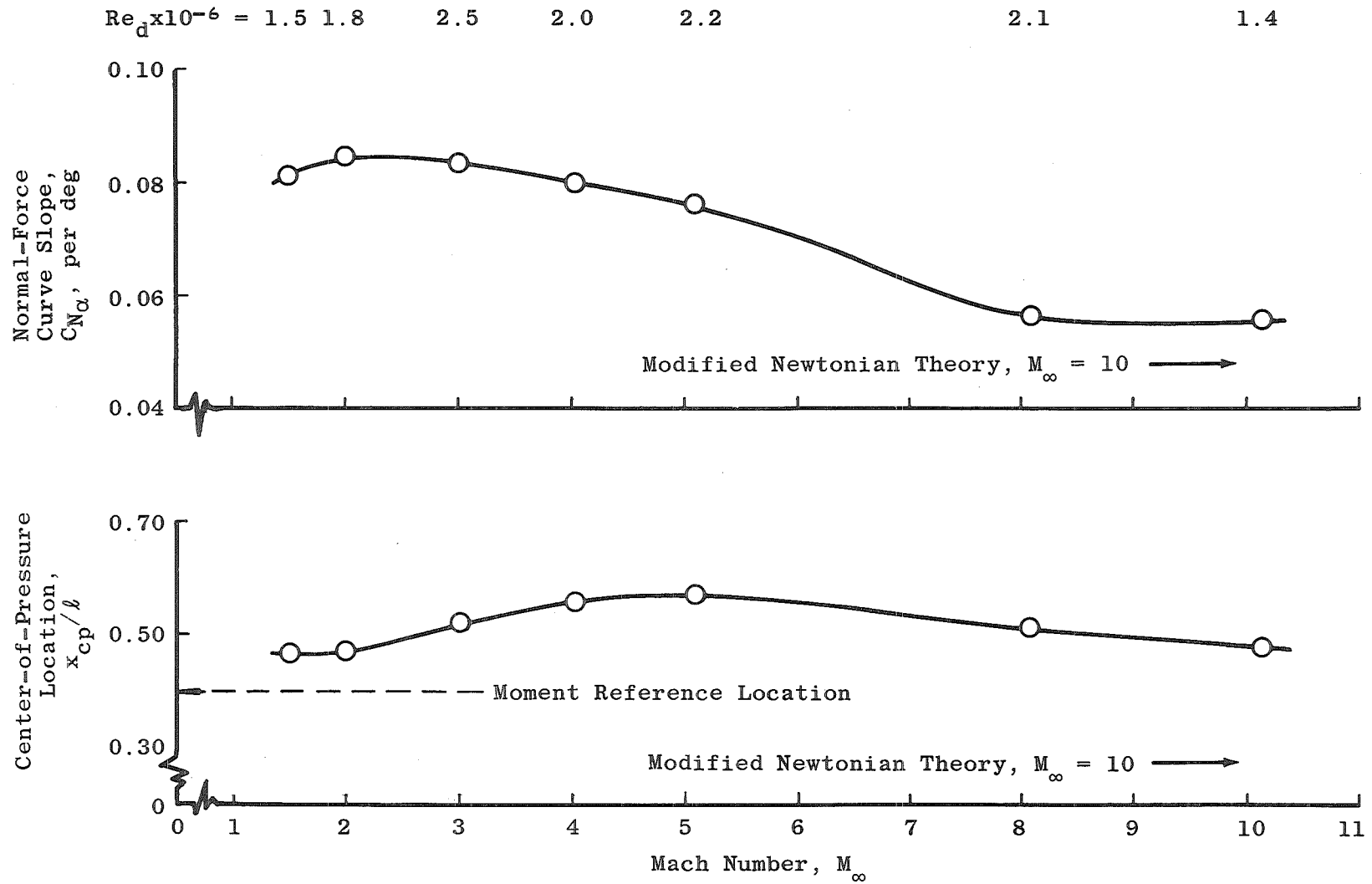
b. Configuration HB-2

Fig. 9 Concluded



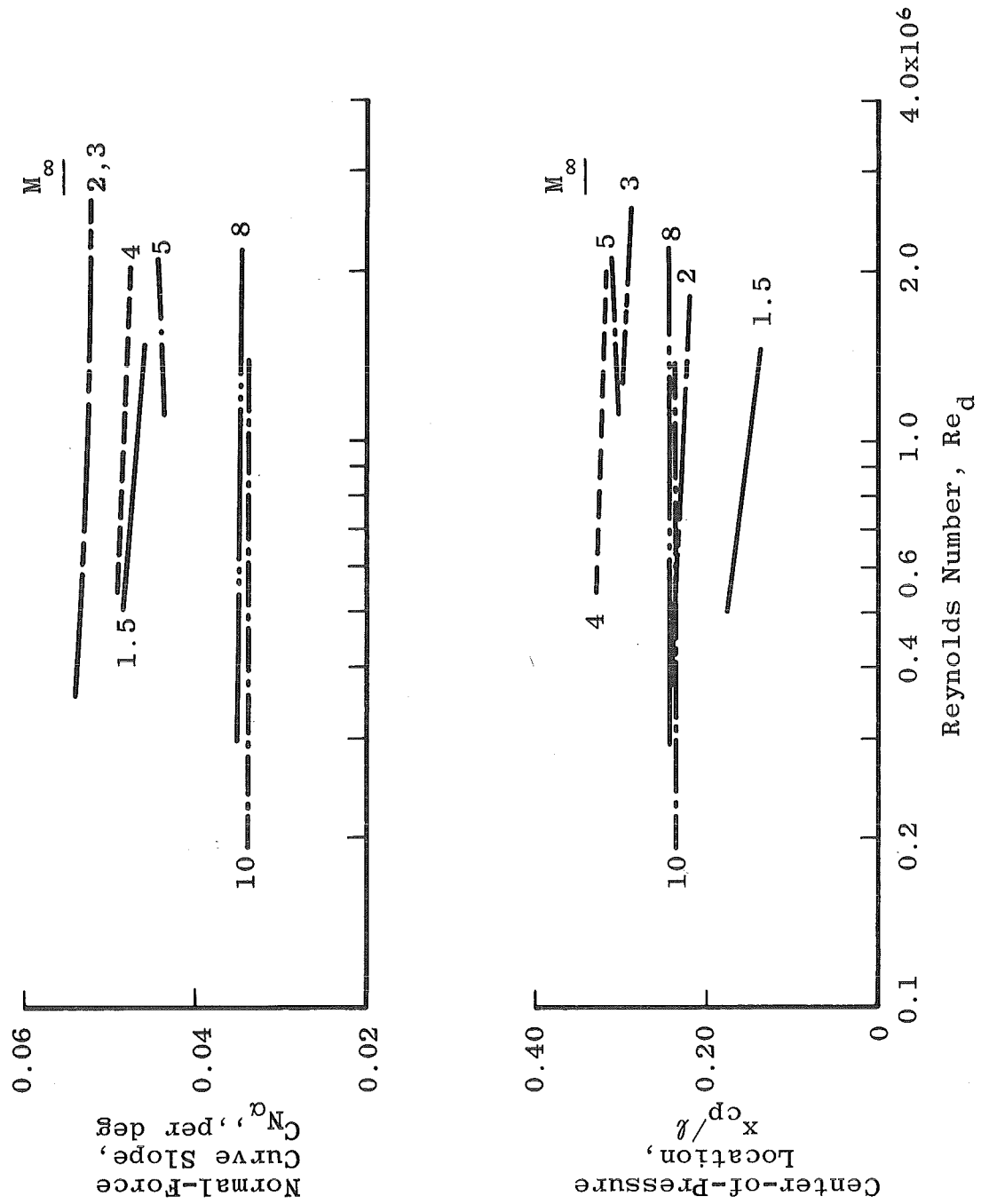
a. Configuration HB-1

Fig. 10 Mach Number Effect on Stability Parameters at Maximum Reynolds Number

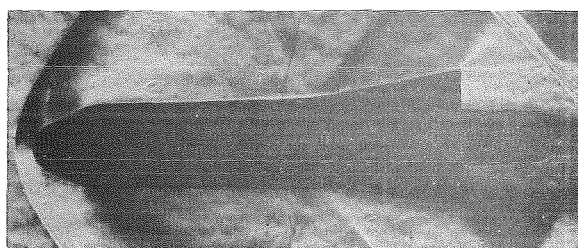


b. Configuration HB-2

Fig. 10 Concluded

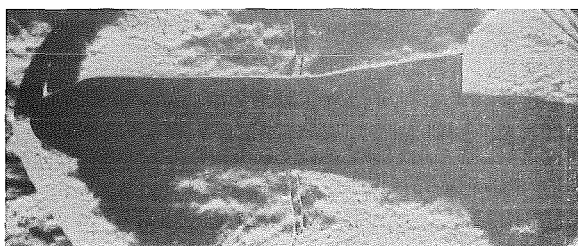


a. Configuration HB-1
 Fig. 11 Reynolds Number Effect on Stability Parameters




$$\text{Re}_d \times 10^{-6} =$$

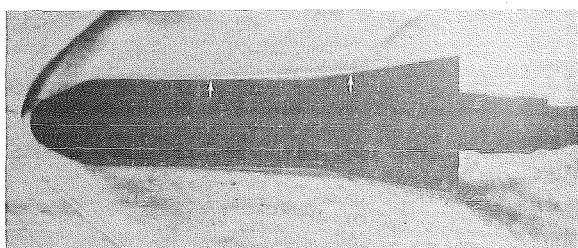
0.18



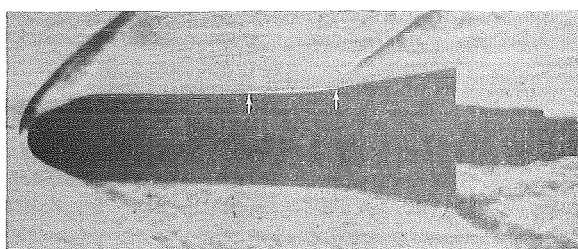
0.70

$$M_\infty = 1.5$$

Note:  Denotes Region of Boundary Layer Separation

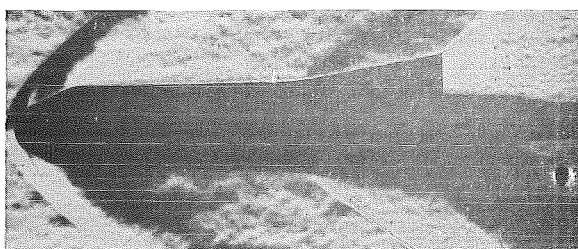


0.11



0.22

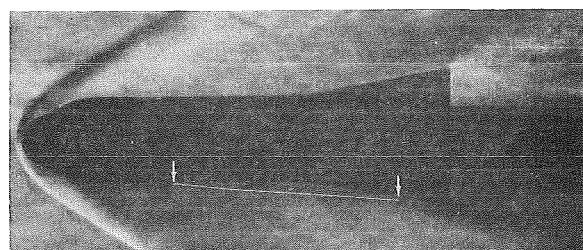
$$M_\infty = 2.0$$



1.11

a. $M_\infty = 1.5$ and 2

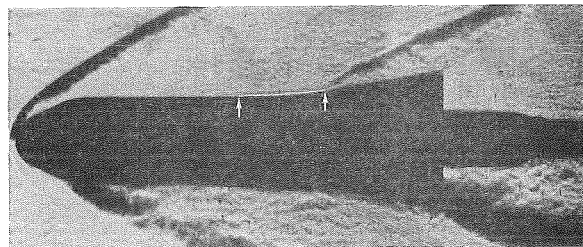
Fig. 12 Schlieren Photographs of HB-2 at Supersonic Speeds ($d = 1.25$ in.)



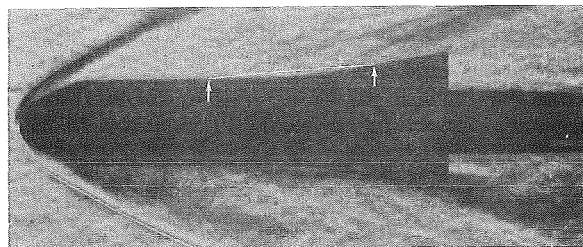
$$Re_d \times 10^{-6} =$$

0.11

$$M_{\infty} = 3$$

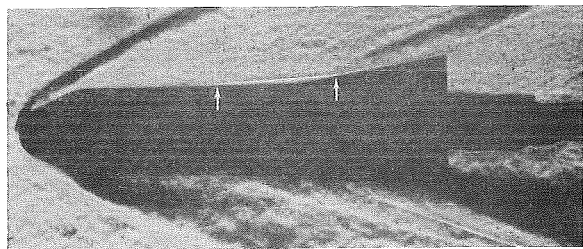


0.67

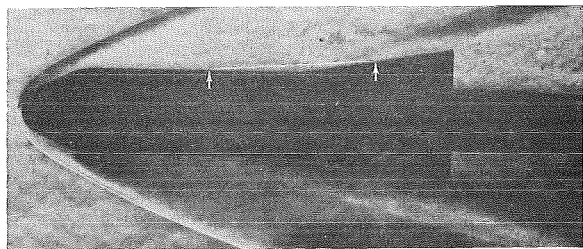


0.31

$$M_{\infty} = 4$$



0.60



0.36

$$M_{\infty} = 5$$

b. $M_{\infty} = 3, 4, \text{ and } 5$

Fig. 12 Concluded